

## Crystal structure refinements of borate dimorphs inderite and kurnakovite using $^{11}\text{B}$ and $^{25}\text{Mg}$ nuclear magnetic resonance and DFT calculations

BING ZHOU,<sup>1,2</sup> VLADIMIR K. MICHAELIS,<sup>3,†</sup> YUANMING PAN,<sup>4</sup> YEFENG YAO,<sup>5</sup> KIMBERLY T. TAIT,<sup>6</sup> BRENDT C. HYDE,<sup>6</sup> JOHN E.C. WREN,<sup>3</sup> BARBARA L. SHERRIFF,<sup>7</sup> AND SCOTT KROEKER<sup>3,\*</sup>

<sup>1</sup>Qinghai Institute of Salt Lakes, Chinese Academy of Sciences, Xining 810008, China

<sup>2</sup>College of Materials Science and Engineering, Tongji University, Shanghai 21000 China

<sup>3</sup>Department of Chemistry, University of Manitoba, Winnipeg, Manitoba R3T 2N2, Canada

<sup>4</sup>Department of Geological Sciences, University of Saskatchewan, Saskatoon, Saskatchewan S7N 5E2, Canada

<sup>5</sup>Physics Department and Shanghai Key Laboratory of Magnetic Resonance, East China Normal University, Shanghai 200062, China

<sup>6</sup>Department of Natural History, Mineralogy, Royal Ontario Museum, Toronto, Ontario M5S 2C6, Canada

<sup>7</sup>Department of Geological Sciences, University of Manitoba, Winnipeg, Manitoba R3T 2N2, Canada

### ABSTRACT

Borate minerals composed of  $[\text{B}\phi_3]$  triangles and/or  $[\text{B}\phi_4]$  tetrahedra ( $\phi = \text{O}$  or  $\text{OH}$ ) commonly exhibit complex polymerizations to form diverse polyanion groups. High-resolution solid-state magic angle spinning (MAS)  $^{11}\text{B}$  and  $^{25}\text{Mg}$  NMR spectroscopy at moderate to ultrahigh magnetic fields (9.4, 14.1, and 21.1 T) allows for very accurate NMR parameters to be obtained for the borate dimorphs, inderite, and kurnakovite,  $[\text{MgB}_3\text{O}_3(\text{OH})_5 \cdot 5\text{H}_2\text{O}]$ . Improved agreement between experimental results and ab initio density functional theory (DFT) calculations using Full Potential Linear Augmented Plane Wave (FP LAPW) with WIEN2k validates the geometry optimization procedures for these minerals and permits refinements of the hydrogen positions relative to previous X-ray diffraction crystal structures. In particular, the optimized structures lead to significant improvements in the positions of the H atoms, suggesting that H atoms have significant effects on the  $^{11}\text{B}$  and  $^{25}\text{Mg}$  NMR parameters in inderite and kurnakovite. This study shows that combined high-resolution NMR spectroscopy and ab initio theoretical modeling provides an alternative method for the refinement of crystal structures, especially H positions.

**Keywords:** Borate dimorphs, saline lakes in Tibet,  $^{11}\text{B}$  NMR,  $^{25}\text{Mg}$  NMR, solid-state NMR, ultrahigh field NMR, ab initio calculations, FC LAPW, NMR crystallography

### INTRODUCTION

Inderite and kurnakovite are hydrated magnesium borate dimorphs mainly found in saline lake sediments in Tibet, California, and the Inder Deposit in Kazakhstan (Corazza 1974, 1976). The fundamental building block in these dimorphs is the tetraborate polyanion in the form of a hexagonal sorborate ring, which is connected with a hydrated Mg-O octahedron to form the rare, charge-neutral  $\text{Mg}(\text{H}_2\text{O})_4\text{B}_3\text{O}_3(\text{OH})_5$  molecular complex (Wan and Ghose 1977). Both dimorph unit cells contain a free water molecule and the  $\text{Mg}(\text{H}_2\text{O})_4\text{B}_3\text{O}_3(\text{OH})_5$  molecular complexes, which are linked together via hydrogen bonds to form three-dimensional structures. The major difference between the dimorphs lies in the linkage of the  $\text{Mg}(\text{H}_2\text{O})_4\text{B}_3\text{O}_3(\text{OH})_5$  complex: in inderite it consists of the tetraborate ring and  $\text{Mg}(\text{OH})_2(\text{H}_2\text{O})_4$  octahedron sharing two OH groups to form discrete molecules, whereas kurnakovite is composed of alternating tetraborate rings and  $\text{Mg}(\text{OH})_2(\text{H}_2\text{O})_4$  octahedra sharing one oxygen atom to form infinite chains (Fig. 1). Therefore, the dimorphs of kur-

nakovite and inderite, which are common borates of economic significance in the saline lakes of Tibet, not only provide an unique opportunity for detailed nuclear magnetic resonance (NMR) studies to shed new insights into the local structures of fundamental building blocks in borates, but are important for better understanding of borate mineralization and dynamics in the modern saline lakes in Tibet.

NMR is useful in probing subtle structural differences between polymorphs (Enright et al. 2007; Harris et al. 2007). However, a solid-state  $^{11}\text{B}$  NMR spectroscopic study of inderite and kurnakovite by Petch et al. (1962) failed to provide any local structural details that are not available from X-ray crystallography. In this study we combine high-resolution  $^{11}\text{B}$  and  $^{25}\text{Mg}$  solid-state MAS NMR spectroscopy at high (14.1 T) and ultrahigh (21.1 T) magnetic fields with ab initio theoretical calculations to better understand the local geometry and investigate the effects of such structural characteristics on the NMR parameters.

$^{11}\text{B}$  and  $^{25}\text{Mg}$  isotopes are quadrupolar nuclei with nuclear spins of  $I = 3/2$  and  $5/2$ , respectively. This enables us to use the quadrupole interactions (QI), which can be described by using the quadrupolar coupling constant ( $C_Q$ ) and the asymmetry parameter ( $\eta$ ), to withdraw structural information. These parameters are related to the principal elements of the electric field gradient (EFG) tensor at the site (Slichter 1992):

\* E-mail: scott\_kroeker@umanitoba.ca

† Present address: Francis Bitter Magnet Laboratory and Department of Chemistry, Massachusetts Institute of Technology, Cambridge, MA 02139, U.S.A.

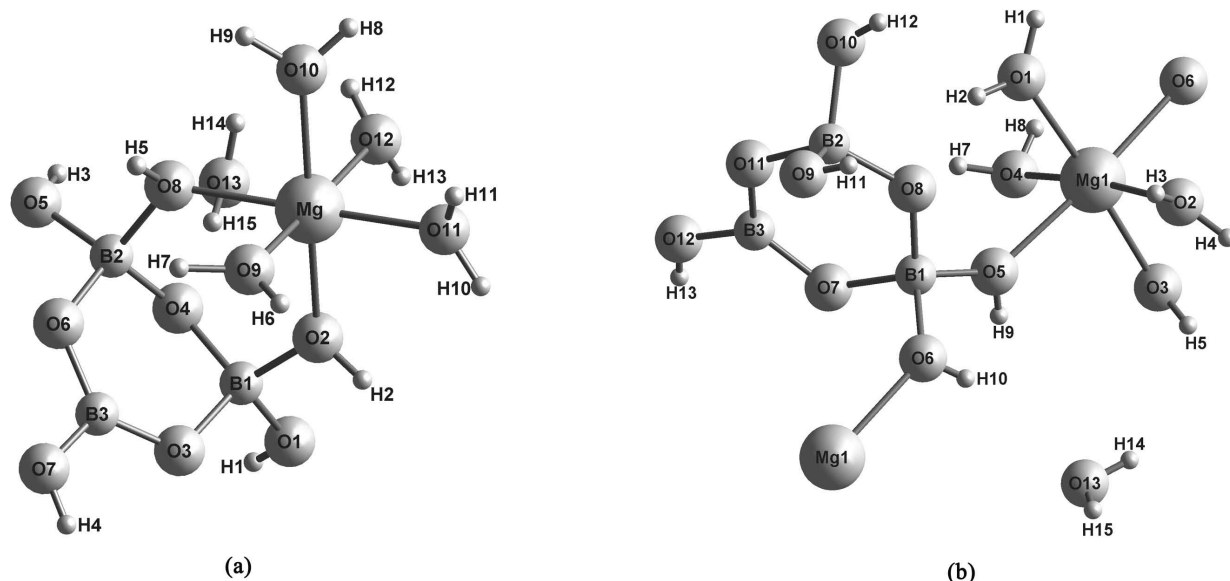


FIGURE 1. Structures of the dimorphs (a) inderite and (b) kurnakovite.

$$C_Q = eV_{zz}Q/h \quad (1)$$

$$\eta = \frac{|V_{xx} - V_{yy}|}{V_{zz}} \quad (2)$$

where  $V_{zz}$ ,  $V_{yy}$ , and  $V_{xx}$  are the EFG components in the principal axis system that fulfills the condition  $|V_{zz}| \geq |V_{yy}| \geq |V_{xx}|$ ,  $e$  is the fundamental charge,  $h$  is Planck's constant, and  $Q$  is the quadrupole moment.

Theoretical Full Potential Linear Augmented Plane Wave (FP LAPW) modeling has gained popularity for the calculation and prediction of electronic and other properties in solids with periodic boundary conditions (Winkler et al. 1996; Bryant et al. 1999; Sherriff and Zhou 2004; Zhou and Sherriff 2004; Zhou et al. 2005, 2007; Hansen et al. 2005). For this full-potential, all-electron method the exchange and correlation effects are treated in the density functional theory (DFT) using the generalized gradient approximation (GGA). The electronic potential in the unit cell is partitioned into spheres around the nuclei and the interstitial area between the spheres, i.e., the muffin-tin partition. A linear combination of the products of radial functions and spherical harmonics is then used inside the atomic spheres and a planewave expansion is used in the interstitial area as the wavefunctions (Cottenier 2002). Finally, the Kohn-Sham equations (Kohn and Sham 1965) are solved by a linear variation of LAPW and thus the electronic structure can be obtained. These calculations are implemented in the WIEN2k computer package (Blaha et al. 1985, 1988, 1990, 1992, 2001). FP LAPW calculations have proved to be very sensitive to atomic positions within the unit cells (Zhou et al. 2005; Hansen et al. 2005) where only slight differences in structural data will give significant differences in the calculated EFG values. Therefore, DFT calculations may also be applied to refine crystal structures. Such a structural optimization using FP LAPW can be implemented by keeping the experimental lattice parameters fixed but adjusting the in-

ternal atomic coordinates until the system energy and the forces acting on all atoms in the unit cell reach a minimum (Zhou et al. 2005; Hansen et al. 2005). This contribution demonstrates that by coupling precisely determined NMR parameters of  $C_Q$  and  $\eta$  (for  $^{11}\text{B}$  and  $^{25}\text{Mg}$ ) with DFT calculations using WIEN2k, significant improvements to the crystal structures from previous XRD studies can be realized. In particular, determination of the positions of all H atoms in the dimorphs inderite and kurnakovite have been refined.

## EXPERIMENTAL METHODS

### Materials

Two sets of inderite and kurnakovite dimorphs from different regions were studied: the saline lakes in Tibet (provided by Mianping Zheng, Chinese Academy of Geological Sciences) and Boron, California (provided by the Royal Ontario Museum). The Tibet specimens are colorless and transparent with a vitreous luster, and have an average grain size of 2 mm. The California specimens are also colorless and transparent with a vitreous luster; however, these samples contain larger crystals. The inderite (M34418) is found in sprays of crystals up to 9 cm long and a few millimeters across. The kurnakovite sample (M23739) is a chunk of massive material, an average grain size is difficult to determine. After handpicking under a binocular microscope, samples were prepared for powder XRD and solid-state NMR experiments.

### Nuclear magnetic resonance

All spectra were acquired at room temperature (298 K). Prior to experiments, the magic angle was adjusted by optimization of the line widths of the spinning sidebands (ssbs) in the  $^{23}\text{Na}$  MAS NMR spectrum of  $\text{NaNO}_3$ , while stable spinning frequencies were achieved by using a rotor-speed controller. Samples were ground to a fine powder (ca. 30–50  $\mu\text{m}$ ) with an agate mortar and pestle, and packed into either 3.2 or 4 mm (outer diameter) zirconia rotors (22 or 80  $\mu\text{L}$  fill volume, respectively) containing sample masses between 35 and 90 mg.

**$^{25}\text{Mg}$  NMR.**  $^{25}\text{Mg}$  NMR spectra were acquired using Bruker Avance II 900 (21.1 T) and Bruker Avance III 400 (9.4 T) spectrometers with 4 mm Bruker double-resonance (DR) MAS probes. Powdered samples were placed into 4 mm (outer diameter) zirconia rotors (80  $\mu\text{L}$  fill volume) accommodating sample masses between 70 and 90 mg. Spectra acquired at 21.1 T used spinning frequencies of 10 kHz, 6000 co-added transients, and 5 s recycle delays with either a quadrupole

echo (Davis et al. 1976) or Bloch-decay sequence ( $\nu_{rf} = 28$  kHz). Lower field (9.4 T) spectra were acquired with a spinning frequency of 13.5 kHz, 64 000 and 96 000 co-added transients, and a 3  $\mu$ s solid pulse width ( $\pi/2$ ). Spectra were externally referenced with respect to 1 M MgCl<sub>2</sub> at 0 ppm.

**<sup>11</sup>B NMR (14.1 T).** Spectra were acquired using a Varian UNITYInova 600 (14.1 T) spectrometer on a 3.2 mm double resonance Varian-Chemagnetics probe (H/F-X) with  $\nu_{rf}$  of 79 kHz and a 0.2  $\mu$ s pulse (tip angle of 7°) at a Larmor frequency of 192.4 MHz. Bloch-decay spectra were acquired with 64 and 4096 co-added transients and optimized recycle delays using a spinning frequency of 6000 and 16000  $\pm$  3 Hz. This data table was zero-filled to 8 K points and multiplied by an exponential function corresponding to 10 to 100 Hz of line broadening before Fourier transformation. Spectra were referenced externally with respect to BF<sub>3</sub>·Et<sub>2</sub>O (0.0 ppm) using 0.1 M boric acid (H<sub>3</sub>BO<sub>3</sub>) at +19.6 ppm as a secondary standard. Due to the abundance of protons in these samples, <sup>1</sup>H decoupling ( $\nu_{rf} = 80$  kHz) was applied during the acquisition; however subsequent comparison between spectra with and without decoupling revealed no effects on the lineshape.

**<sup>11</sup>B NMR (21.1 T).** <sup>11</sup>B MAS NMR data were collected with a short tip angle ( $\sim 10^\circ$ ) using a single-pulse experiment, 128 co-added transients, and a spinning frequency of 18 kHz. Recycle delays were optimized and were found to be 5 s. Spectra were externally referenced with respect to BF<sub>3</sub>·Et<sub>2</sub>O (0.0 ppm) using 0.1 M boric acid (+19.6 ppm) as a secondary standard.

### DFT calculations

FP LAPW calculations were implemented using the WIEN2k software package. Atomic coordinates and space groups for the dimorphs of kurnakovite and inderite from Corazza (1974, 1976) were used as input files. The following atomic-sphere radii (RMT), given in atomic units (a.u.), were used so that the calculations ran with the highest efficiency without core charge leakage: H(0.45/0.6), B(1.2/1.3), O(1.3/1.4), and Mg(1.7). The core electron states were separated from the valence states at  $-6.0$  Ry. Calculations were performed at a planewave cutoff defined by  $\min(\text{RMT})\text{-max}(\text{Kn}) = 2.5$ , where Kn is the k vector corresponding to approximately 10 000 plane waves for the dimorphs. In all calculations, the irreducible Brillouin zone was sampled on shifted tetrahedral meshes at 32 k-points, which can achieve good convergence, as expected for insulators. Angular momentum components up to  $l = 12$  were included for the wavefunctions inside the atomic spheres. The self-consistent calculations were run in a non-spin-polarized mode and the convergence conditions of the self-consistent cycles were set at  $5 \times 10^{-5}$  Ry. For the minimization procedure, the force convergence condition at each atom was set to 1 mRy/a.u. To make a comparison between the structures optimized with all atoms and with only H atoms, the structures were independently optimized for all atoms or for only the H atoms while keeping the other atoms at fixed positions. CIFs for optimized structures have been deposited as supporting online material<sup>1</sup>. The DFT structure optimizations typically required 16 steps. All of the WIEN2k calculations were performed on a multi-node cluster of computers (16 nodes with total 256 cores) at the Shanghai Super Computer Center with the Quad-Core AMD Opteron Processor 2350 at 2 GHz and 1024 GB RAM. The quadrupolar moment used for the <sup>11</sup>B calculations was 0.0409 barn (Hansen et al. 2005).

CASTEP utilizes the Perdew-Burke-Ernzerhof functional, GGA for the exchange-correlation energy and ultrasoft pseudopotentials (Profeta et al. 2003; Perdew et al. 1996). Calculations were performed using a fine-accuracy basis set and a maximum planewave energy of 550 eV. The Monkhorst-Pack grid had a maximum density of up to  $3 \times 3 \times 8$  k-points. CASTEP software was used in the Materials Studio 4.4 environment, with all calculations conducted on an HP xw4400 workstation with a single Intel Dual-Core 2.67 GHz processor and 8 GB DDR RAM. Quadrupolar couplings and asymmetry parameters were calculated using identical crystal coordinates (vide supra, Corazza) and hydrogen geometry optimization.

### NMR spectral simulation

Simulations of <sup>11</sup>B MAS NMR central transition line shapes and spinning sideband manifolds were performed using the STARS software package (Skibsted et al. 1991) under conditions of ideal excitation. Parameters for three-coordinate boron peaks were principally determined by fitting the central-transition lineshape, with peaks from satellite transitions serving as additional checks on the accuracy of the fit. WSolids (Eichele and Wasylishen 2001) was also used to simulate the three-coordinate boron central transition lineshapes under the approximation of “infinite” spinning speed to assist in evaluating the experimental uncertainty. Due to the lack of observable second-order quadrupolar effects on the central transition for four-coordinate boron, high-quality <sup>11</sup>B MAS NMR spectra of the spinning sideband manifold were collected and modeled using STARS to obtain  $\delta_{iso}$ ,  $C_Q$ , and  $\eta$ . Values for  $C_Q$  and  $\eta$  obtained from ab initio theoretical calculations were

taken as the initial input for the simulations, then  $\delta_{iso}$ ,  $C_Q$ , and  $\eta$  were optimized by manual adjustments to achieve agreement with the experimental <sup>11</sup>B spectra. The robustness of the resulting fits was tested by varying the parameters independently. Estimated uncertainties in the cited parameters were obtained by visually inspecting the agreement between calculated and experimental spectra and the “goodness of fit” for variation of a given parameter, with, and without attempts to compensate for the changes by reasonable modifications of the other parameters. All NMR data were fitted independently at multiple fields, providing additional constraints and verifying the accuracy and precision of the derived parameters.

### Powder X-ray diffraction

X-ray diffraction analysis for the California samples used a Bruker D8 Advance with Da Vinci design, at the Royal Ontario Museum. This system employed a CuK $\alpha$  source running at 40 kV and 40 mA and a LynxEye detector. Small amounts of representative powder were dusted onto a low background plate and the samples were scanned in steps of 0.01° from 10 to 70° 2 $\theta$ . Diffraction data have been deposited as supporting online material<sup>1</sup>.

For the Tibet specimens, sample purity was confirmed using a PANalytical X'Pert Pro Bragg-Brentano powder X-ray diffractometer with a CuK $\alpha$  radiation source, an X'Celerator detector and a Ni-filter diffracted beam. Data were acquired at room temperature with a 2 $\theta$  range of 10° to 60° at 0.0167° increments using 60 s per step.

## RESULTS AND DISCUSSION

The <sup>11</sup>B MAS NMR spectra for the dimorphs at 14.1 and 21.1 T are illustrated in Figures 2 and 3. Both sets of dimorphs (i.e., Tibet and California) yielded the same NMR parameters. Although there are two crystallographically distinct <sup>11</sup>B sites in the structures of inderite and kurnakovite, only a single resonance at  $\sim 1$  ppm is observed in the 14.1 T data, undoubtedly due to the similar structural environments and the small chemical shift range for <sup>11</sup>B in borates (Turner et al. 1986; Kroeker and Stebbins 2001; Müller et al. 1993). The 21.1 T data reveal a hint of asymmetry in the <sup>11</sup>B peaks, possibly because of greater chemical shift dispersion at high field. The full-width at half maximum of these peaks is essentially identical at both fields due to the negligible second-order quadrupole effect in the highly symmetrical pseudotetrahedral environment. We have employed all possible means (e.g., fast MAS and high-power proton decoupling) to achieve the highest possible resolution in the tetrahedral region. Further information can sometimes be gained by close examination of the satellite transition spinning sideband peaks, however no additional evidence of multiple sites with different quadrupolar parameters could be detected.

The central transition of the <sup>11</sup>B site (12 to 20 ppm) shows a typical second-order quadrupolar lineshape (Figs. 2 and 3). The 21.1 T data provide cleaner edges and a narrower CT lineshape due to the reduction of second-order quadrupole effects, yielding increased resolution. The complementary multifield data enable better definition of the NMR parameters in the associated spectral simulations than with a single magnetic field. The best-fit NMR parameters are given in Table 1.

<sup>25</sup>Mg has a moderate quadrupolar moment (19.94 fm<sup>2</sup>) and a low gyromagnetic ratio  $\gamma$  ( $-1.6388 \times 10^7$  rad T<sup>-1</sup> s<sup>-1</sup>) that places its receptivity relative to <sup>1</sup>H at  $2.68 \times 10^{-4}$ . The <sup>25</sup>Mg MAS NMR spectra for the dimorphs at 21.1 T show second-order quadrupolar

<sup>1</sup> Deposit item AM-12-083, supplementary information and CIFs. Deposit items are available two ways: For a paper copy contact the Business Office of the Mineralogical Society of America (see inside front cover of recent issue) for price information. For an electronic copy visit the MSA web site at <http://www.minsocam.org>, go to the *American Mineralogist* Contents, find the table of contents for the specific volume/issue wanted, and then click on the deposit link there.

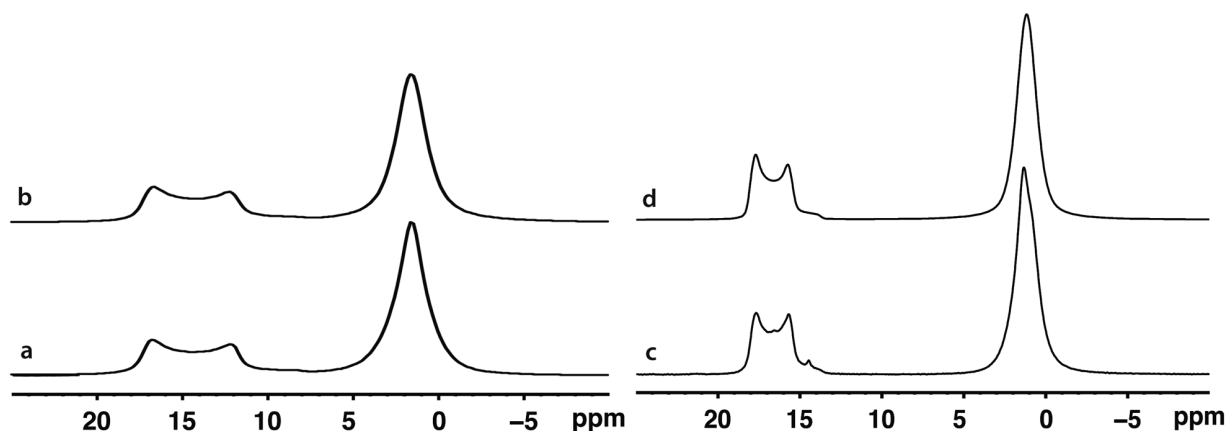


FIGURE 2. Experimental (a and c) and simulated (b and d)  $^{11}\text{B}$  MAS NMR spectra of inderite at 14.1 T (a and b) and 21.1 T (c and d).

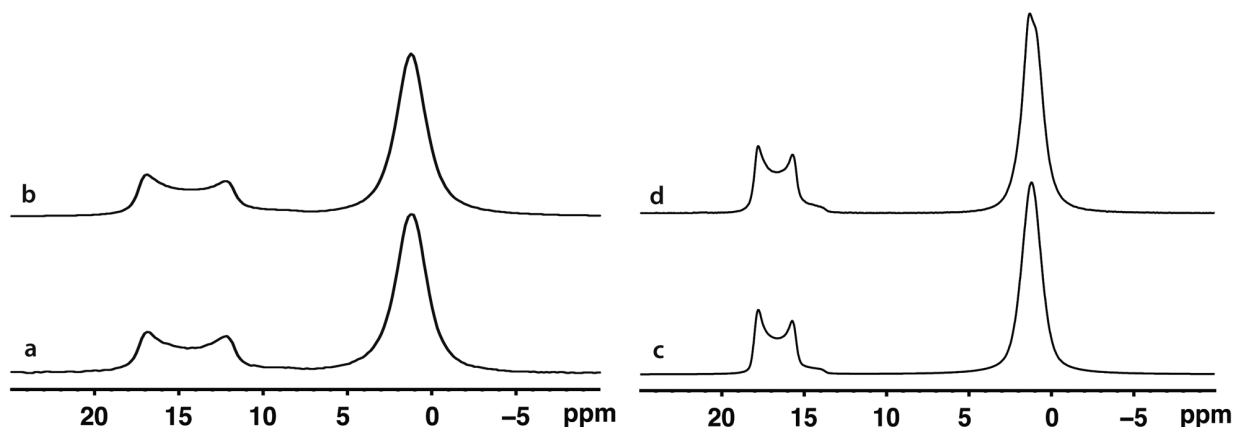


FIGURE 3. Experimental (a and c) and simulated (b and d)  $^{11}\text{B}$  MAS NMR spectra of kurnakovite at 14.1 T (a and b) and 21.1 T (c and d).

lineshapes for the single Mg sites, with good signal-to-noise for a traditionally difficult NMR nucleus (Fig. 4). The  $^{25}\text{Mg}$  NMR parameters obtained from spectral simulations are listed in Table 1.

The theoretical  $^{25}\text{Mg}$   $C_Q$  and  $\eta$  values ( $-5.095$  MHz and 0.23) of kurnakovite calculated from the original structure of Corazza (1974) using WIEN2k differ from the experimental results (4.5

MHz and 0.30) by approximately 13 and 22%, respectively (Table 1). These values calculated by CASTEP ( $-5.927$  MHz and 0.18) differ by as much as 32 and 40%, respectively (Table 1). At the same time, the calculated  $C_Q$  values at the  $^{13}\text{B}$  site from the XRD structure of kurnakovite by WIEN2k and CASTEP differ from the experimental one by 4 and 19%, respectively, and much

TABLE 1. Experimental and calculated NMR results for kurnakovite and inderite

	Experimental NMR			Theoretical calculations									
	$\delta_{\text{iso}}$	$C_Q$	$\eta$	CASTEP <sup>3</sup>		CASTEP <sup>4</sup>		WIEN2k <sup>3</sup>		WIEN2k <sup>4</sup>		WIEN2k <sup>5</sup>	
				$C_Q$	$\eta$	$C_Q$	$\eta$	$C_Q$	$\eta$	$C_Q$	$\eta$	$C_Q$	$\eta$
<b>Kurnakovite</b>													
$^{61}\text{Mg}^2$	3(2)	4.5(1)	0.30(3)	-5.927	0.18	-5.270	0.13	-5.095	0.23	-4.779	0.18	-4.564	0.33
$^{13}\text{B}^1$	18.7(1)	2.52(2)	0.09(3)	2.989	0.12	3.000	0.09	2.413	0.13	2.506	0.10	2.498	0.098
$^{10}\text{B}(1)^1$				0.689	0.37	0.598	0.96	-0.583	0.3	-0.514	0.99	0.567	0.86
$^{10}\text{B}(2)^1$	1.63(5)	0.58(3)	0.5(3)	0.427	0.94	0.458	0.63	0.401	0.86	0.429	0.57	0.372	0.47
<b>Inderite</b>													
$^{61}\text{Mg}^2$	0(2)	4.3(2)	0.35(5)	5.065	0.42	4.684	0.21	4.301	0.41	4.354	0.36	4.385	0.36
$^{13}\text{B}^1$	18.9(1)	2.55(2)	0.03(3)	2.966	0.08	2.963	0.06	2.418	0.084	2.474	0.06	2.462	0.064
$^{10}\text{B}(1)^1$				0.493	0.33	0.512	0.24	0.391	0.38	0.419	0.26	0.432	0.22
$^{10}\text{B}(2)^1$	1.29(5)	0.52(3)	0.5(3)	0.380	0.96	0.283	0.92	0.328	0.99	0.315	0.95	-0.230	0.95

<sup>1</sup> Determined from 14.1 and 21.1 T experimental data using simulation software STARS and WSolids (see text for details).

<sup>2</sup> Determined from 9.4 and 21.1 T experimental data using simulation software STARS and WSolids (see text for details).

<sup>3</sup> Calculated results from the XRD atomic coordinates of Corazza (1974, 1976).

<sup>4</sup> Calculated results from structural optimizations involving only H atoms.

<sup>5</sup> Calculated results from structural optimizations for all atoms.

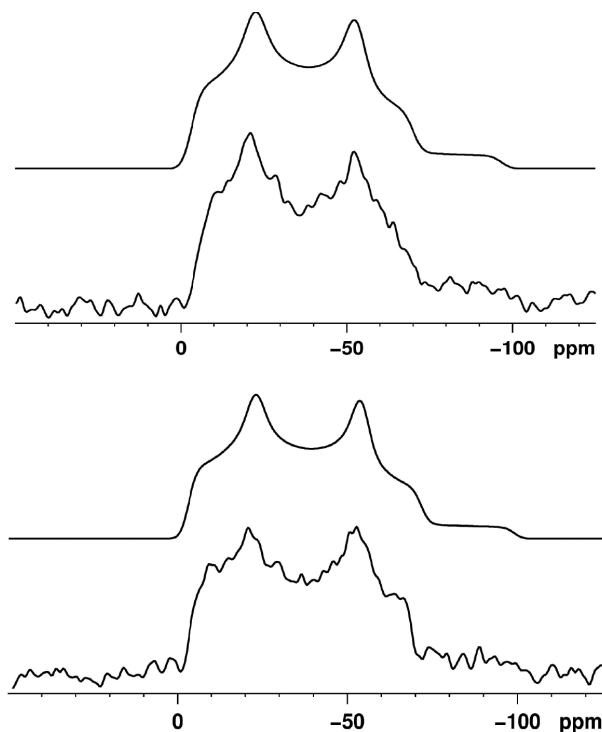


FIGURE 4. Experimental and simulated  $^{25}\text{Mg}$  MAS NMR for inderite (top) and kurnakovite (bottom) at 21.1 T.

more for  $\eta$ . Similarly, smaller but still significant discrepancies exist between the experimental NMR parameters and the theoretically calculated results for Mg and B in inderite if the XRD structure of Corazza (1976) is used for theoretical calculations. For example, for the  $^{13}\text{B}$  site in inderite, the calculated  $C_Q$  values using WIEN2k and CASTEP differ from the experimental result by  $\sim 5$  and  $\sim 16\%$ , respectively, although the calculated  $\eta$  values from both methods are close to the experimental result. On the other hand, the  $^{25}\text{Mg}$   $C_Q$  and  $\eta$  values calculated by CASTEP using the inderite XRD structure deviate from the experimental ones by 18 and 20%, respectively, with differences of 3 and 17% when compared with those from WIEN2k. As for the  $^{14}\text{B}$  sites in the dimorphs, all the calculated  $C_Q$  values by both CASTEP and WIEN2k are less than 0.7 MHz, in congruence with the experimental results. The  $\eta$  values for the  $^{14}\text{B}$  sites are not tightly constrained from theoretical calculations owing to the small EFG components (Table 1) (see Eq. 2).

These significant discrepancies in the  $^{11}\text{B}$  and  $^{25}\text{Mg}$   $C_Q$  and  $\eta$  values between the NMR experiments and theoretical calculations (Table 1) suggest the need for better atomic coordinates than those available from previous XRD studies. Accordingly, we performed partial (hydrogen positions only) and full DFT geometry optimizations for the crystal structures of inderite and kurnakovite using WIEN2k. Optimizations resulted in a decrease of the forces on each of the 32 atoms in the unit cells of both inderite and kurnakovite from the average value of 567 mRy/a.u. (with the maximum of 1514 mRy/a.u.) in the original XRD structures to only 1 mRy/a.u. The optimized fractional atomic coordinates resulting from these calculations are compared with

the original XRD data of Corazza (1974, 1976) in Tables 2 and 3.

After full optimization the calculated  $C_Q$  and  $\eta$  values for the Mg site in kurnakovite differ from the experimental results by only 2% and 10%, respectively. The calculated  $C_Q$  and  $\eta$  values for the  $^{13}\text{B}$  site in the optimized kurnakovite structure are also in better agreement with the experimental values (Table 1); the change in  $\eta$  for  $^{13}\text{B}$  is more pronounced than that for  $C_Q$ . The sign of the quadrupolar coupling for the  $^{14}\text{B}(1)$  site in kurnakovite changed after the optimization, but the  $\eta$  values for the  $^{14}\text{B}$  sites remain poorly constrained due to the fact that the small EFG tensor components are close to each other (Table 1). The  $C_Q$  and  $\eta$  values of the  $^{13}\text{B}$  and Mg sites in inderite after optimization are systematically closer to the experimental ones than those from the XRD data (Table 1), albeit not as dramatically as those observed for kurnakovite. For example, the discrepancies for  $C_Q$  at both the  $^{13}\text{B}$  and Mg sites in inderite are reduced to only 2% after structural optimization. The calculated  $^{11}\text{B}$   $C_Q$  value of 0.43 MHz for  $^{14}\text{B}(1)$  site in inderite is also close to the value of 0.52 MHz determined from the experimental spectra. These improvements are particularly significant when considering that  $^{11}\text{B}$   $C_Q$  and  $\eta$  typically change very little with geometric distortion (Bray et al. 1961; Turner et al. 1986; Kroeker and Stebbins 2001).

The WIEN2k calculations appear to more closely match the experimental data for unoptimized and partially optimized structures than the analogous CASTEP data (Table 1), and hence we devote the remainder of the discussion to WIEN2k results. Tables 2 and 3 show that the optimized positions of the Mg, O, and B atoms usually differ from the XRD ones of Corazza (1974)

TABLE 2. Comparison of optimized fractional atomic coordinates for kurnakovite from WIEN2k and XRD results (in parentheses)

Atom	x/a	y/b	z/c
Mg	0.6528 (0.653)	0.2316 (0.2321)	0.8025 (0.8015)
B1	0.7677 (0.769)	0.2268 (0.2274)	0.3519 (0.3509)
B2	0.1134 (0.1105)	0.3524 (0.3529)	0.501 (0.5008)
B3	0.9826 (0.9826)	0.1041 (0.1053)	0.3049 (0.3116)
O1	0.9241 (0.9215)	0.3174 (0.3212)	0.9219 (0.9191)
O2	0.5995 (0.5943)	0.4121 (0.4091)	0.7839 (0.7761)
O3	0.3820 (0.3833)	0.1344 (0.1349)	0.6676 (0.6685)
O4	0.6690 (0.6697)	0.0326 (0.0351)	0.8086 (0.8077)
O5	0.6481 (0.6506)	0.1899 (0.1926)	0.4728 (0.4737)
O6	0.6699 (0.6713)	0.2660 (0.2632)	0.1446 (0.1415)
O7	0.8091 (0.8096)	0.1016 (0.103)	0.2650 (0.2675)
O8	0.9346 (0.9334)	0.3330 (0.3339)	0.5103 (0.5057)
O9	0.1495 (0.1496)	0.4436 (0.4402)	0.3556 (0.3546)
O10	0.2562 (0.2496)	0.4046 (0.4093)	0.7360 (0.7348)
O11	0.1301 (0.1284)	0.2212 (0.2214)	0.4054 (0.413)
O12	0.0150 (0.016)	0.9859 (0.9886)	0.2400 (0.2486)
O13	0.2845 (0.2869)	0.2375 (0.2434)	0.0414 (0.0522)
H1	0.0134 (0.994)	0.3732 (0.359)	0.0767 (0.06)
H2	0.9681 (0.964)	0.3341 (0.335)	0.7999 (0.81)
H3	0.6644 (0.668)	0.4713 (0.473)	0.7108 (0.736)
H4	0.4765 (0.491)	0.4172 (0.42)	0.7496 (0.745)
H5	0.2939 (0.314)	0.1711 (0.174)	0.5762 (0.597)
H6	0.3141 (0.328)	0.0478 (0.058)	0.6853 (0.695)
H7	0.7732 (0.752)	0.0227 (0.027)	0.7737 (0.76)
H8	0.7067 (0.702)	0.0395 (0.039)	0.9742 (0.942)
H9	0.5346 (0.562)	0.1154 (0.137)	0.3744 (0.399)
H10	0.5483 (0.59)	0.2595 (0.266)	0.1377 (0.145)
H11	0.1176 (0.128)	0.5248 (0.498)	0.4018 (0.406)
H12	0.2710 (0.261)	0.4973 (0.483)	0.8089 (0.796)
H13	0.9048 (0.937)	0.9058 (0.926)	0.1446 (0.186)
H14	0.2463 (0.263)	0.2616 (0.257)	0.1663 (0.159)
H15	0.2725 (0.269)	0.3050 (0.298)	0.9512 (0.973)

Note: The XRD atomic coordinates and lattice constants ( $a = 8.3479 \text{ \AA}$ ,  $b = 10.6068 \text{ \AA}$ ,  $c = 6.4447 \text{ \AA}$ ,  $\alpha = 98.846^\circ$ ,  $\beta = 108.981^\circ$ ,  $\gamma = 105.581^\circ$ ) are from the single-crystal XRD study of Corazza (1974).

**TABLE 3.** Comparison of optimized fractional atomic coordinates for nderite from WIEN2k and XRD results (in parentheses)

Atom	x/a	y/b	z/c
Mg	0.25580 (0.25554)	0.21609 (0.21593)	0.11712 (0.11712)
O1	0.68893 (0.68846)	0.14501 (0.14513)	0.43403 (0.43446)
O2	0.49876 (0.49914)	0.20999 (0.20971)	0.25488 (0.25525)
O3	0.76657 (0.76635)	0.08601 (0.08591)	0.25799 (0.25799)
O4	0.45440 (0.45422)	0.03557 (0.03518)	0.30381 (0.30389)
O5	0.27859 (0.27814)	0.89012 (0.88970)	0.20256 (0.20271)
O6	0.54467 (0.54471)	0.96387 (0.96394)	0.13889 (0.13879)
O7	0.86290 (0.86228)	0.99229 (0.99248)	0.10921 (0.10960)
O8	0.23439 (0.23444)	0.05827 (0.05904)	0.11602 (0.11597)
O9	0.42417 (0.42303)	0.20598 (0.20585)	0.99209 (0.99206)
O10	0.98823 (0.98898)	0.21769 (0.21720)	0.98619 (0.98621)
O11	0.27635 (0.27596)	0.37166 (0.37071)	0.10488 (0.10495)
O12	0.07032 (0.06975)	0.23141 (0.23179)	0.23703 (0.23651)
O13	0.15583 (0.15545)	0.02164 (0.02048)	0.41011 (0.41014)
B1	0.59932(0.59920)	0.11862 (0.11845)	0.31359 (0.31376)
B2	0.37941 (0.37922)	0.98750 (0.98747)	0.19273 (0.19274)
B3	0.72300 (0.72279)	0.01672 (0.01671)	0.17058 (0.17064)
H1	0.7391 (0.730)	0.0860 (0.096)	0.4838 (0.479)
H2	0.5831 (0.577)	0.2726 (0.263)	0.2697 (0.271)
H3	0.1920 (0.2040)	0.8944 (0.8910)	0.2556 (0.2480)
H4	0.9966 (0.9740)	0.0282 (0.0250)	0.1250 (0.1250)
H5	0.2112 (0.2140)	0.0348 (0.0430)	0.0346 (0.0410)
H6	0.5134 (0.4930)	0.2606 (0.2530)	0.9758 (0.9750)
H7	0.4456 (0.4420)	0.1452 (0.1430)	0.9469 (0.9510)
H8	0.8799 (0.8930)	0.2716 (0.2620)	0.9715 (0.9740)
H9	0.9289 (0.9400)	0.1640 (0.1650)	0.9305 (0.9330)
H10	0.3876 (0.3820)	0.4182 (0.4120)	0.1418 (0.1400)
H11	0.2187 (0.2180)	0.4045 (0.3970)	0.0285 (0.0340)
H12	0.9566 (0.9670)	0.1856 (0.1920)	0.2410 (0.2360)
H13	0.1412 (0.1290)	0.2451 (0.2450)	0.3171 (0.3060)
H14	0.0215 (0.0360)	0.0384 (0.0330)	0.3600 (0.3660)
H15	0.2620 (0.2500)	0.0374 (0.0300)	0.3673 (0.3720)

Note: The XRD atomic coordinates and lattice constants ( $a = 6.8221 \text{ \AA}$ ,  $b = 13.1145 \text{ \AA}$ ,  $c = 12.0350 \text{ \AA}$ ,  $\beta = 104.552^\circ$ ) are from the single-crystal XRD study of Corazza (1976).

in the third decimal point for kurnakovite and the fourth decimal for nderite. However, such changes for the B and Mg atoms in kurnakovite are minor because even the largest variations are only 0.2 and 2.66%, respectively. As for the coordinates for all O atoms in kurnakovite, generally the change is below 3%, except 20.21% for the z-coordinate of O13, 7.08% for the y-coordinate of O4, and 6.2% for the x-coordinate of O12. Therefore, the most significant coordinate change for O atoms in kurnakovite occurs in the free water molecule (O13), and the second is O12 coordinated to the  $^{13}\text{B}$  site. The optimized bond distances between B, Mg, and O atoms are listed in Table 4, which shows that the optimized B and Mg polyhedra in both dimorphs are more regular than those reported in previous XRD studies.

For the 15 H atoms in kurnakovite, 10 (H1–H10) are in the form of water molecules and are coordinated to the Mg–O octahedron, two (H14 and H15) are in the free water molecule, and the three remaining hydrogen atoms (H11, H12, and H13) are coordinated to B in the form of OH. Compared with the XRD structure of Corazza (1974), the changes in the coordinates for the 15 H atoms in kurnakovite after structural optimization are more dramatic than those of the O, B, and Mg atoms, with differences occurring in the second decimal point. H1, H6, H7, H9, and H13 are among the most significant changes and the maximum change is 98.6% for the x-coordinate of H1. As a result, the calculated  $^{25}\text{Mg}$  NMR parameters from the optimized structures differ dramatically, because its 4 H atoms (H1, H7, H9, and H10) and one O atom (O4) show significant coordinate differences. Similarly, the large  $C_Q$  change at the  $^{14}\text{B}$ 1 site is

**TABLE 4.** Comparison of nonhydrogen bond distances ( $\text{\AA}$ ) between WIEN2k and XRD for kurnakovite and nderite

Bond	Kurnakovite		Inderite	
	WIEN2k	XRD	WIEN2k	XRD
Mg–O1	2.0232	2.0070	2.0307	2.036
Mg–O2	2.0908	2.0804	2.0743	2.062
Mg–O3	2.0305	2.0230	2.1146	2.110
Mg–O4	2.1565	2.1368	2.0900	2.086
Mg–O5	2.0879	2.0820	2.0530	2.042
Mg–O6	2.1294	2.1134	2.1555	2.152
Mean	2.0864	2.0738	2.0864	2.081
B1–O5	1.4653	1.4636	1.4663	1.469
B1–O6	1.5060	1.4962	1.4705	1.467
B1–O7	1.5298	1.5118	1.5220	1.522
B1–O8	1.4595	1.4439	1.4559	1.458
Mean	1.4902	1.4789	1.4787	1.479
B2–O8	1.4374	1.4490	1.4501	1.449
B2–O9	1.4868	1.4689	1.4697	1.475
B2–O10	1.4948	1.4801	1.4677	1.470
B2–O11	1.4940	1.4873	1.4948	1.501
Mean	1.4783	1.4713	1.4706	1.474
B3–O7	1.3782	1.3708	1.3651	1.364
B3–O11	1.3750	1.3619	1.3684	1.367
B3–O12	1.3836	1.3709	1.3830	1.377
Mean	1.3789	1.3679	1.3722	1.369

accompanied by the changed O6 and H9 atoms. On the other hand, the change in  $C_Q$  for the second  $^{14}\text{B}$ (2) site is small, because the positions of its immediate neighbor O and H atoms change little after optimization. The  $^{13}\text{B}$  site is also accompanied by large changes in O12 and H13, thus resulting in significant improvements in the calculated  $^{11}\text{B}$  NMR parameters at this site after structural optimization.

Rather than the optimization of all 32 atoms in the unit cell of kurnakovite, optimization of only the 15 hydrogen atoms was also attempted by WIEN2k and CASTEP, but this yielded essentially the same results as above, except that H13 changes more dramatically.

The positions of the B, Mg, and O atoms in nderite are almost unchanged (less than 1%) after optimization, except for a 5% change in the y-coordinate of O10, thus verifying the closely related quadrupolar parameters for  $^{25}\text{Mg}$  and  $^{11}\text{B}$  using both XRD and optimized structures. As in kurnakovite, the H atoms in nderite change dramatically: H15 (23%), H14 (40%), H5 (19%), H11 (16%), and H1 (10%), where H14 and H15 are in the free water molecule. Also similar to kurnakovite, the three atoms (O10, H11, and H5) with changes over 5% are coordinated to the Mg octahedron, whereas H1 is close to B1. Not surprisingly, the calculated  $C_Q$  and  $\eta$  from the optimized structures are systematically in better agreement with experimental results than those from the XRD structure (Table 1).

These results consistently show that the atomic coordinates in both dimorphs most affected by DFT optimization are the 15 H atoms. This is attributable to the large uncertainty in the location of H atoms by X-ray diffraction due to the non-spherical nature of the electron density and the small diffraction coefficient of this atom (Hansen et al. 2005; Burns and Hawthorne 1993, 1994). Another contributing factor may be the disorder (i.e., dynamic behavior) of H or static disorder in the crystal structures, so that the H positions (especially those in molecular water) are very difficult to determine by X-rays, and XRD studies generally give only average positions. Therefore, the H positions obtained from XRD usually lead to inaccurate O–H bond distances (Table 5), which are commonly significantly shorter than those obtained

by the more reliable neutron diffraction. This problem is well known in XRD studies of borates and has been addressed by the use of theoretical calculations (Burns and Hawthorne 1993, 1994; Sun et al. 2011). In the present work, the reproduction of highly accurate experimental NMR parameters by structural optimization of DFT calculations provides an alternate way to refine H positions in minerals.

After structural optimization, the distances between the O13 atom of the free water molecule and its four neighboring H atoms in kurnakovite become 0.9816, 0.9959, 1.7781, and 2.0198 Å (Table 5). The water molecule in the optimized structure shows stronger hydrogen bonding indicated by the shorter O13-O10 and H1-O9 distances (2.8434 vs. 2.8910 Å and 1.6974 vs. 1.82 Å). Shorter distances between O1 and O9 through H1 (1.6977 vs. 1.8236 Å) and between O6 and O2 through H12 (2.3756 and 2.4083 vs. 2.5357 and 2.5482 Å) also indicate stronger hydrogen bonding. Thus, molecular water exerts a greater influence on the structure than suggested by previous XRD studies.

The sign of  $C_Q$ , seldom available from NMR experiments (Menger and Veeman 1982; Kroeker et al. 1999), can be obtained by theoretical calculations and provides additional information about the electronic structure around the nucleus investigated. The FP LAPW calculations using the original XRD structures (Corazza 1974, 1976) show both positive and negative signs for  $C_Q$  of the two  $^{14}\text{B}$  sites in kurnakovite [−0.58 MHz for  $^{14}\text{B}(1)$ , 0.40 MHz for  $^{14}\text{B}(2)$ ], but are all positive for  $^{14}\text{B}$  sites in inderite (Table 1). However, the optimized structure for kurnakovite gives positive signs for  $C_Q$  at both  $^{14}\text{B}$  sites (Table 1). The different sign for  $C_Q$  is due to the highest charge density being along the Z direction for one  $^{14}\text{B}$  site and the lowest charge density along Z for the other  $^{14}\text{B}$  site (i.e., oblate vs. prolate shape) in the XRD structure. After structural optimization, the charge density characteristics of the two  $^{14}\text{B}$  sites in kurnakovite agree. Similarly, the calculated sign of  $C_Q$  for the Mg site is negative in kurnakovite but positive in inderite. This indicates that the

local Mg coordination environments in the dimorphs are different, in that they share one or two O atoms with the neighboring triborate ring in kurnakovite and inderite, respectively (Corazza 1974, 1976). Also, the Mg octahedron in inderite consists of two OH and two water molecules in the equatorial plane, whereas its counterpart in kurnakovite contains four water molecules in the equatorial plane (Fig. 1). As a result, there is a slight elongation shown by the diagonal distance of 2.131 Å between O9-O12 compared with 2.057 Å for the other four distances (Table 3) in the Mg octahedron of inderite. This is in a sharp contrast with the oblate shape in kurnakovite, indicated by the diagonal O5-O6 distance of 2.4197 Å compared with 2.9406 Å for the other four distances (Table 2). This explains the different  $C_Q$  signs for  $^{25}\text{Mg}$  in the dimorphs.

In summary, solid-state NMR experiments at 14.1 and 21.1 T provide accurate NMR parameters for inderite and kurnakovite, two important borates. By combining high-resolution solid-state  $^{11}\text{B}$  and  $^{25}\text{Mg}$  MAS NMR spectroscopy with DFT calculations, the crystal structures of these dimorphs have been improved. The NMR parameters calculated from the optimized crystal structures provide superior agreement with the  $^{25}\text{Mg}$  and  $^{11}\text{B}$  NMR experimental results compared to those calculated from the original XRD structures. In particular, the positions of H atoms two bonds away have a significant impact on the  $^{11}\text{B}$  and  $^{25}\text{Mg}$  quadrupolar parameters, making this combination a sensitive structural tool. This demonstration of “NMR crystallography” is particularly valuable for the refinement of H atomic positions, which are notoriously difficult to obtain using X-ray diffraction.

## ACKNOWLEDGMENTS

B.Z. received a research grant from the “One Hundred People Plan,” Chinese Academy of Sciences. Additional funding has been provided by the Canada Foundation for Innovation, Natural Sciences and Engineering Research Council of Canada [Discovery Grant (S.K.); PGSD3 (V.K.M.)] and the Government of Manitoba. Y.Y. acknowledges financial support from NSFC grant no. 21174039. The authors thank S.R. Giesbrecht, and B.J. Greer for helpful discussions, and Victor V. Tersikh for assistance at the Ultrahigh-Field NMR facility. Access to the 900 MHz NMR spectrometer was provided by the National Ultrahigh-Field NMR Facility for Solids (Ottawa, Canada), a national research facility funded by the Canada Foundation for Innovation, the Ontario Innovation Trust, Recherche Quebec, the National Research Council Canada, and Bruker BioSpin and managed by the University of Ottawa (www.nmr900.ca). The Natural Sciences and Engineering Research Council of Canada (NSERC) is acknowledged for a Major Resources Support grant. The careful attention and insightful comments of the reviewers are appreciated.

## REFERENCES CITED

- Blaha, P., Schwarz, K., and Herzig, P. (1985) First-principles calculation of the electric field gradient of  $\text{Li}_3\text{N}$ . *Physical Review Letters*, 54, 1192–1195.
- Blaha, P., Schwarz, K., and Dederichs, P.H. (1988) First-principles calculation of the electric field gradient in hcp metals. *Physical Review B*, 37, 2792–2796.
- Blaha, P., Schwarz, K., and Sorantin, P. (1990) Full potential linearized augmented plane wave programs for crystalline systems. *Computational Physics Communication*, 59, 39–415.
- Blaha, P., Singh, D.J., Sorantin, P.I., and Schwarz, K. (1992) Electric-field-gradient calculations for systems with large extended-core-state contributions. *Physical Review B*, 46, 1321–1325.
- Blaha, P., Schwarz, K., Madsen, G.K., Kvasnicka, D., and Luitz, J. (2001) WIEN2k, an augmented plane wave+local orbitals program for calculating crystal properties. *Karlsruhe Schwarz, Technische Universität Wien, Vienna*.
- Bray, P., Edwards, J., O’Keefe, J., Ross, V., and Tatsuzaki, I. (1961) Nuclear magnetic resonance studies of  $^{11}\text{B}$  in crystalline borates. *Journal of Physical Chemistry*, 35, 435–442.
- Bryant, P.L., Harwell, C.R., Wu, K., and Fronczek, F.R. (1999) Single-crystal  $^{27}\text{Al}$  NMR of andalusite and calculated electric field gradients: the first complete NMR assignment for a 5-coordinate aluminum site. *Journal of Physical Chemistry*, 103, 5246–5252.
- Burns, P.C. and Hawthorne, F.C. (1993) Hydrogen bonding in colemanite: an X-ray

**TABLE 5.** Comparison of hydrogen bond distances (Å) between WIEN2k and XRD (shown in parentheses) for kurnakovite and inderite

Donor	Hydrogen bond		Distance		
	H atoms	Acceptor	D-A	D-H	H-A
<b>Kurnakovite</b>					
O1	H2	O8	2.7098 (2.721)	0.9911 (0.89)	1.7903 (1.90)
O2	H3	O9	2.7339 (2.754)	0.9936 (0.91)	1.7898 (1.87)
O2	H4	O10	2.7605 (2.803)	0.9974 (0.86)	1.7792 (1.97)
O3	H6	O7	2.7697 (2.774)	0.9883 (0.89)	1.7832 (1.88)
O4	H7	O12	2.8119 (2.832)	0.9944 (0.86)	1.8269 (2.00)
O5	H9	O4	2.8507 (2.888)	0.9895 (0.76)	1.8629 (2.13)
O6	H10	O13	2.9888 (3.012)	0.9855 (0.70)	2.022 (2.33)
O9	H11	O8	2.4416 (2.769)	0.9996 (0.74)	1.7423 (2.03)
O10	H12	O2	3.0476 (3.074)	0.9799 (0.79)	2.4086 (2.54)
O12	H13	O13	2.7730 (2.864)	1.0009 (0.74)	1.7738 (2.14)
O13	H14	O11	3.0267 (3.035)	0.9816 (0.78)	2.1081 (2.29)
O13	H15	O10	2.8434 (2.891)	0.9959 (0.84)	1.8619 (2.06)
<b>Inderite</b>					
O1	H1	O13	2.8891 (2.889)	0.9003 (0.84)	1.9895 (2.05)
O2	H2	O5	2.7843 (2.784)	0.9160 (0.87)	1.8724 (1.92)
O5	H3	O7	3.0858 (3.086)	0.8962 (0.83)	2.8230 (2.8)
O7	H4	O8	2.6669 (2.667)	0.9074 (0.85)	1.8098 (1.86)
O9	H6	O1	2.8654 (2.865)	0.9016 (0.84)	1.9682 (2.03)
O10	H8	O1	2.6851 (2.684)	0.9157 (0.86)	1.7721 (1.82)
O10	H9	O5	2.8935 (2.893)	0.9556 (0.94)	2.0295 (2.04)
O12	H13	O10	3.2580 (3.258)	0.9045 (0.85)	2.5919 (2.62)
O13	H14	O3	2.9485 (2.947)	0.9146 (0.87)	2.0419 (2.08)
O13	H15	O4	2.6706 (2.671)	0.9277 (0.89)	1.7478 (1.79)

- and structure-energy study. *Canadian Mineralogist*, 31, 297–304.
- (1994) Kaliborite: an example of a crystallographically symmetrical Hydrogen bond. *Canadian Mineralogist*, 32, 885–894.
- Corazza, E. (1974) The crystal structure of kurnakovite: a refinement. *Acta Crystallographica*, B30, 2194–2199.
- (1976) Inderite: crystal structure refinement and relationship with kurnakovite. *Acta Crystallographica*, B32, 1329–1333.
- Cottenier, S. (2002) Density functional theory and family of (L)APW-methods: a step-by-step introduction. Instituut voor Kern-en Stralingsfysica, K.U. Leuven, Belgium.
- Davis, J.H., Jeffrey, K.R., Bloom, M., Valic, M.I., and Higgs, T.P. (1976) Quadrupolar echo deuteron magnetic resonance spectroscopy in ordered hydrocarbon chains. *Chemical Physics Letters*, 42, 390–394.
- Eichele, E. and Wasylshen, R.E. (2001) WSOLIDS NMR Simulation Package, Version 1.17.30. Dalhousie University, Halifax.
- Enright, G.D., Tersikh, V.V., Brouwer, D.H., and Ripmeester, J.A. (2007) The structure of two anhydrous polymorphs of caffeine from single-crystal diffraction and ultrahigh-field solid-state  $^{13}\text{C}$  NMR spectroscopy. *Crystal Growth and Design*, 7, 1406–1410.
- Hansen, M.R., Madsen, G.K., Jakobsen, H.J., and Skibsted, J. (2005) Refinement of Borate structures from  $^{11}\text{B}$  MAS NMR spectroscopy and density functional theory calculations of  $^{11}\text{B}$  electric field gradients. *Journal of Physical Chemistry A*, 109, 1989–1997.
- Harris, R.K., Cadars, S., Emsley, L., Yates, J.R., Pickard, C.J., Jetti, R.K.R., and Griesser, U.J. (2007) NMR crystallography of oxybuprocaine hydrochloride, Modification II. *Physical Chemistry Chemical Physics*, 9, 360–368.
- Kohn, W. and Sham, L.J. (1965) Self-consistent equation including exchange and correlation effects. *Physical Review*, 140(4A), 1133–1138.
- Kroeker, S. and Stebbins, J.F. (2001) Three-coordinated Boron-11 chemical shifts in borates. *Inorganic Chemistry*, 40, 6239–6246.
- Kroeker, S., Wasylshen, R.E., and Hanna, J.V. (1999) The structure of solid copper(I) cyanide: A multinuclear magnetic and quadrupole resonance study. *Journal of American Chemistry Society*, 121, 1582–1590.
- Menger, E.M. and Veeman, W.S. (1982) Quadrupole effects in high-resolution phosphorus-31 solid-state NMR spectra of triphenylphosphine copper (I) complexes. *Journal of Magnetic Resonance*, 46, 257–268.
- Müller, D., Grimmer, A.R., Timper, U., Heller, G., and Shakibaie-Moghadam, M.Z. (1993)  $^{11}\text{B}$ -MAS-NMR-Untersuchungen zur Anionenstruktur von Boraten. *Zeitschrift für anorganische und allgemeine Chemie*, 619, 1262–1268.
- Perdew, J.P., Burke, K., and Ernzerhof, M. (1996) Generalized gradient approximation made simple. *Physical Chemical Letters*, 77, 3865–3868.
- Petch, H.E., Pennington, K.S., and Cuthbert, J.D. (1962) On Christ's postulated boron-oxygen polyions in some hydrated borates of unknown crystal structure. *American Mineralogist*, 47, 401–404.
- Profeta, M.M., Mauri, F., and Pickard, C.J. (2003) Accurate first principles prediction of  $^{17}\text{O}$  NMR parameters in  $\text{SiO}_2$ : assignment of the zeolite ferrierite spectrum. *Journal of American Chemical Society*, 125, 541–548.
- Sherriff, B.L. and Zhou, B. (2004)  $^{29}\text{Si}$  and  $^{23}\text{Na}$  MAS NMR spectroscopic study of penkvilksite  $\text{Na}_4\text{Ti}_2\text{Si}_6\text{O}_{22}\cdot 5\text{H}_2\text{O}$ . *Canadian Mineralogist*, 42, 1027–1035.
- Skibsted, J., Nielsen, N., Bildsøe, H., and Jakobsen, H. (1991) Satellite transitions in MAS spectra of quadrupolar nuclei. *Journal of Magnetic Resonance*, 95, 117–132.
- Slichter, C.P. (1992) *Principles of Magnetic Resonance*. Springer-Verlag, Berlin.
- Sun, W., Huang, Y.-X., Li, Z., Pan, Y., and Mi, J.-X. (2011) Hydrothermal synthesis and single-crystal X-ray structure refinement of three borates: sibirskite, parasibirskite and priceite. *Canadian Mineralogist*, 49, 823–834.
- Turner, G.L., Smith, K.A., Kirkpatrick, R.J., and Oldfield, E. (1986) Boron-11 nuclear magnetic resonance spectroscopic study of borate and borosilicate minerals and a borosilicate glasses. *Journal of Magnetic Resonance*, 67, 544–550.
- Wan, C. and Ghose, S. (1977) Hungchaoite,  $\text{Mg}(\text{H}_2\text{O})_3\text{B}_4\text{O}_5(\text{OH})_4\cdot 2\text{H}_2\text{O}$ : a hydrogen-bonded molecular complex. *American Mineralogist*, 62, 1135–1143.
- Winkler, B., Blaha, P., and Schwarz, K. (1996) Ab initio calculation of electric-field-gradient tensors of forsterite. *American Mineralogist*, 81, 545–549.
- Zhou, B. and Sherriff, B.L. (2004) Quantum calculations of the electronic structure and NMR quadrupolar interaction parameters for tugtupite. *American Mineralogist*, 89, 377–381.
- Zhou, B., Giavani, T., Bildsøe, H., Skibsted, J., and Jakobsen, H. (2005) Structural refinement of  $\text{CsNO}_3(\text{II})$  by coupling of  $^{14}\text{N}$  MAS NMR experiments with WIEN2k DFT calculations. *Chemical Physics Letters*, 402, 133–137.
- Zhou, B., Sherriff, B.L., Hartman, J.S., and Wu, G. (2007)  $^{27}\text{Al}$  and  $^{23}\text{Na}$  NMR spectroscopy and structural modeling of aluminofluoride minerals. *American Mineralogist*, 92, 34–43.

MANUSCRIPT RECEIVED OCTOBER 8, 2011

MANUSCRIPT ACCEPTED JULY 19, 2012

MANUSCRIPT HANDLED BY BRIAN PHILLIPS